

Experimental single-photon exchange along a space link of 7000 km

Daniele Dequal,¹ Giuseppe Vallone,^{1,2} Davide Bacco,¹ Simone Gaiarin,¹ Vincenza Luceri,³
Giuseppe Bianco,⁴ and Paolo Villorosi^{1,2,*}

¹*Dipartimento di Ingegneria dell'Informazione, Università degli Studi di Padova, Padova, Italy*

²*Istituto di Fotonica e Nanotecnologie, CNR, Padova, Italy*

³*e-GEOS spa, Matera, Italy*

⁴*Matera Laser Ranging Observatory, Agenzia Spaziale Italiana, Matera, Italy*

(Received 22 September 2015; published 12 January 2016)

Extending the single-photon transmission distance is a basic requirement for the implementation of quantum communication on a global scale. In this work we report the single-photon exchange from a medium Earth orbit satellite (MEO) at more than 7000 km of slant distance to the ground station at the Matera Laser Ranging Observatory. The single-photon transmitter was realized by exploiting the corner cube retroreflectors mounted on the LAGEOS-2 satellite. Long duration of data collection is possible with such altitude, up to 43 min in a single passage. The mean number of photons per pulse (μ_{sat}) has been limited to 1 for 200 s, resulting in an average detection rate of 3.0 counts/s and a signal-to-noise ratio of 1.5. The feasibility of single-photon exchange from MEO satellites paves the way to tests of quantum mechanics in moving frames and to global quantum information.

DOI: [10.1103/PhysRevA.93.010301](https://doi.org/10.1103/PhysRevA.93.010301)

Introduction. Quantum communications (QC) are necessary for tests on the foundation of quantum physics, such as Bell's inequalities violation [1–3], entanglement swapping [4,5] and distribution [6], and quantum teleportation [7]. Moreover, the transmission of light quanta over long distances is crucial for the realization of several quantum information protocols, such as quantum key distribution (QKD) [8–10], quantum authentication [11], and quantum digital signature [12].

One of the main challenges of QC consists in extending the length of the communication channel, which on ground is nowadays limited to few hundreds of kilometers, both for free space [7] and optical fibers [13]. To overcome these limitations, in the last decade the feasibility of a quantum channel from an orbiting terminal has been explored both theoretically [14–19] and experimentally by exploiting the Ajisai [20] and Champ [21] satellites. Notably, recent transmission of qubits beyond the Earth's atmosphere [22] proved the feasibility of QC from several low Earth orbit (LEO) satellites, within 1500 km of altitude with respect to Earth surface and with typical passage duration of a few minutes. However, proposals for fundamental tests of quantum mechanics with moving frames, involving special and general relativity are based on link distances exceeding the LEO scale [23,24]. Moreover, satellites with orbits higher than LEO are interesting for the implementation of unconditionally secure information protocols for future global navigation satellite system (GNSS) constellations [25] or for the realization of permanent links with geostationary (GEO) satellites.

In this perspective, this work aims at the expansion of QC with higher satellites by realizing the first single-photon exchange spanning a distance exceeding 7000 km, with a mean photon number per pulse leaving the satellite (μ_{sat}) lower than 1 for an extended part of the link and with the single-photon return signal above the noise. Moreover we will show that, with an upgrade of the detector on ground with commercially

available parts, it would be possible to achieve a signal-to-noise-ratio (SNR) suitable for quantum communication up to 23 000 km, corresponding to the distance to GNSS.

Experimental realization. As sketched in the top panel of Fig. 1, to simulate a single-photon source in orbit we exploited a train of light pulses directed towards the LAGEOS-2 satellite and retroreflected by the satellite corner cube retroreflectors (CCRs). Such pulses are attenuated in the uplink by the combined effect of telescope divergence, optical diffraction, atmospheric absorption, and atmospheric turbulence [26]. The mean photon number μ_{sat} of the retroreflected pulses has been estimated by the link budget equation. Because of CCRs backreflection capacity, the ground station is automatically in the illuminated cone on ground.

The pulses are directed towards the satellite by a tracking telescope that is also used as single-photon receiver. The transmitter and receiver setups share the same telescope Coudé path and are combined by a beam splitter (BS). The train of upgoing pulses is generated by a mode-locking Nd:YVO₄ laser oscillator, operating at 1064 nm and with repetition rate stabilized at 100 MHz by an atomic clock. By means of a Periodically Poled Lithium Niobate nonlinear crystal, we obtained pulses at the wavelength of 532 nm, with 1.1 nJ of energy and a duration of 100 ps FWHM. The beam size and divergence are corrected with a Galilean beam expander before entering the Coudé path of the telescope. Finally, the pulses are directed towards the satellite by the 1.5 m diameter primary mirror of the Matera Laser Ranging Observatory (MLRO) of the Italian Space Agency, located in Matera, Italy.

The optical setup for the detection of the single photons from the satellite is composed by a focusing optics, field-of-view (FOV) control, filtering and a single-photon detector, based on a photomultiplier tube (PMT), Hamamatsu H7360-02. The PMT output is time tagged with an 81 ps time resolution by a fast time-to-digital converter (TDC), QuTAU, from QuTOOLS. Two shutters are used to alternate the transmission and reception periods and to avoid the exposure of the PMT to stray upward light. The FWHM of the receiver

*paolo.villorosi@dei.unipd.it

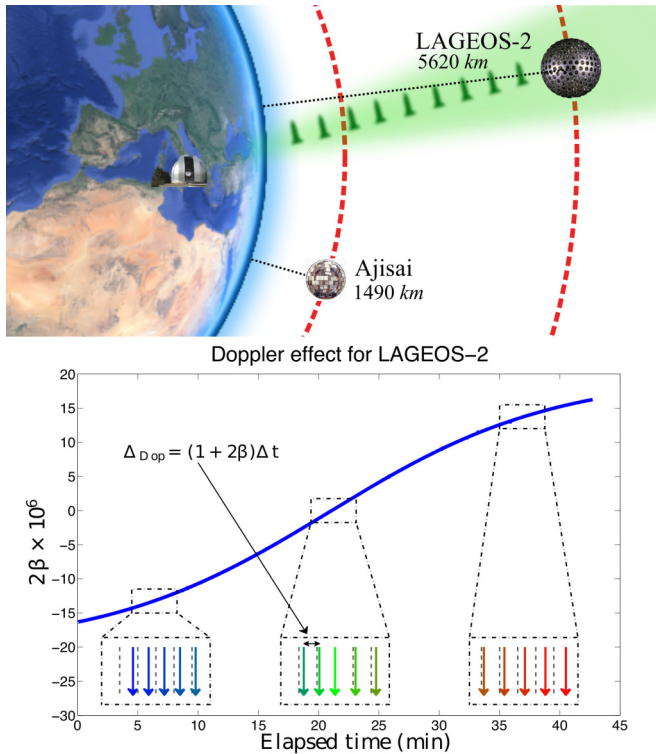


FIG. 1. Top: schematic of the two-way protocol. A pulsed laser beam is directed toward a satellite equipped with CCRs and redirected toward the ground station. The two satellite trajectories are drawn to reproduce the distances in scale of Ajisai and LAGEOS-2 from the Earth's surface. Bottom: measured radial velocity v_R in natural units $\beta = v_R/c$. The corresponding Doppler effect on the pulse separation is schematized on the three boxes: when $\beta < 0$ ($\beta > 0$) the pulse separations at the receiver are smaller (larger) than the transmitted pulse separations. The Doppler effect affects in the same way the 10 Hz SLR beam and the 100 MHz beam used for single-photon generation.

FOV has been set to $100 \mu\text{rad}$ for reducing the gathering of background. In addition, a spectral filter of 3 nm FWHM transmission band around 532 nm has been used to reduce the stray light counts below the 50 counts/s intrinsic dark counts of the PMT.

Temporal synchronization. To discriminate photons received from the satellite from the uncorrelated background, detected events are temporally filtered according to the instantaneous round-trip time of light. Photon expected times of arrival t_{ref} at the receiver are not periodic during the satellite passage, as they depend on the actual distance from the ground station and on the radial velocity of the satellite. The time difference between two consecutive t_{ref} deviates from the period of 10 ns imposed at the generation by a factor $1 + 2v_R/c$, where v_R is the satellite radial velocity and c is the speed of light as shown in Fig. 1 (bottom).

In [20], the t_{ref} 's were obtained by calculating the satellite orbital parameters. Here, similarly to [22], we have introduced an ancillary pulsed beam to simplify the prediction of t_{ref} . Such ancillary beam realizes the satellite laser ranging (SLR) in real time and it is derived from the same oscillator used for the generation of the single-photon train, thus providing an intrinsic

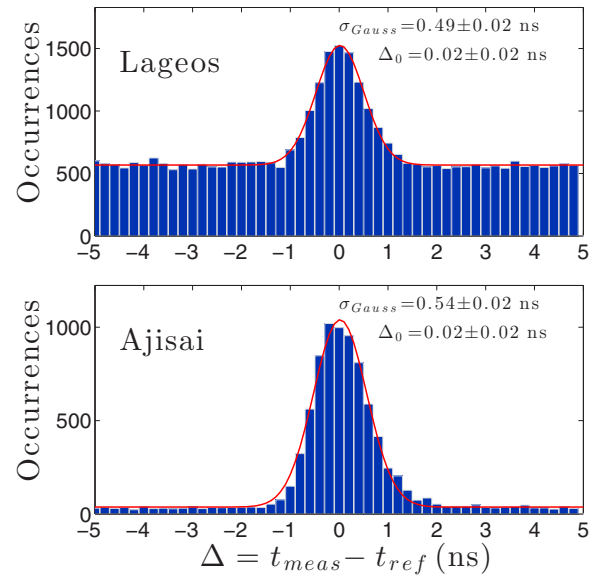


FIG. 2. Comparison of the measured time of detection with the expected time of photon arrival. The compatibility of the fit parameters for LEO and MEO satellites demonstrates the robustness of the analysis method independently from the satellite distance.

temporal synchronization between the two beams. The SLR beam is generated by a three-stage laser amplifier system, and consists of a train of 100 mJ laser pulses with a repetition rate of 10 Hz. It is combined together with the single-photon beam toward and from the satellite. The exit and return instants of the SLR beam are detected using fast photodiodes and time tagged by the same TDC used to register the PMT detections. Since both beams follow the same path to and from the satellite, the actual t_{ref} of every pulse of the 100 MHz train may be obtained in real time and with subnanosecond accuracy by the Doppler effect measured on the SLR signal (Fig. 1, bottom).

We tested the synchronization method with two satellites in different orbits: Ajisai, a LEO satellite with altitude of 1490 km also used in [20,22], and LAGEOS-2, a MEO satellite with altitude of 5620 km. For both satellites, we evaluated the difference of the measured time tags of a complete passage with the nearest t_{ref} calculated by the ancillary SLR pulses. The results are presented in Fig. 2 without any selection on the mean number of photons hitting the satellite: in both cases, a peak exceeding the background was obtained.

We extracted the residual offset (Δ_0) and the standard deviation (σ_G) by Gaussian fitting the distribution of the differences. The residual offset is $\Delta_0 = 0.02 \pm 0.02 \text{ ns}$ in both cases and results compatible with zero, thus demonstrating the validity of this synchronization technique for both the LEO and MEO satellites. The measured standard deviations for the two passages are $0.49 \pm 0.02 \text{ ns}$ for LAGEOS-2 and $0.54 \pm 0.02 \text{ ns}$ for Ajisai. These two values are compatible within the experimental errors, indicating that the synchronization procedure can be effectively used also for larger satellite distance. In both cases, the temporal precision of the single-photon counts is essentially determined by the 0.50 ns jitter of the PMT detectors.

Link budget analysis. The radar equation [26] predicts that the overall link losses, namely, the ratio between the received (f_{rx}) and transmitted (f_{tx}) photon rate, depend on the satellite distance R as follows:

$$\frac{f_{rx}}{f_{tx}} = \alpha G_t \frac{T_a^2(R)}{R^4}, \quad (1)$$

where $\alpha = 237m^4$ is a coefficient that includes optical attenuation, geometrical factors, satellite cross section, and detection efficiency for LAGEOS-2, G_t is the transmission gain, and T_a the one-way atmospheric transmission coefficient.

In (1), the detection rate depends on the instantaneous satellite slant distance R both directly, due to the factor $1/R^4$, and implicitly in T_a , which is given by

$$T_a(R) = T_0^{2R(h_t+R_e)\exp(-h_t/h_s)/[(h_s+R_e)^2-R^2-(h_t+R_e)^2]}, \quad (2)$$

where $T_0 = 0.89$ is the zenith transmission coefficient at sea level, $h_t = 537$ m is the observatory altitude above sea level, $R_e = 6371$ km is the Earth's radius, $h_s = 5620$ km is the satellite altitude, and $h_s = 1.2$ km a scaling factor [26]. We note that the slant distance R is in general larger than the satellite altitude shown in Fig. 1.

We analyzed the entire passage of LAGEOS-2 by dividing it in intervals of 60 s each, in which the mean return rate (\bar{f}_{rx}) was computed. To point out the events to be ascribed to the 100 MHz train from the uncorrelated background, we subtracted from the total detection rate the background rate measured from the events distant more than $6\sigma_G$ from t_{ref} , where σ_G is the standard deviation of the Gaussian fit of Fig. 2.

Figure 3 shows the satellite distance (top) and the \bar{f}_{rx} (middle) as a function of the elapsed time from the beginning of the satellite passage. It is possible to notice a drop in \bar{f}_{rx} between minute 17 and 27. This is due to a larger telescope pointing error near the zenith. With the exclusion of this interval, \bar{f}_{rx} has been fit with (1), leaving as free parameter the transmitter gain $G_t = \frac{8}{\theta_p^2} \exp[-2(\frac{\theta_p}{\theta_t})^2]$, where θ_t is the fixed telescope divergence and θ_p is the time varying pointing error. The result of the fit for the whole passage of LAGEOS-2 is $G_t = (4.7 \pm 0.2) \times 10^8$. Excluding the above-mentioned period, the total photon transmission time was then 32 min, which greatly extends the link durations previously reported [20–22], which were at the level of a few tens of seconds per satellite passage. This is due to two reasons: the duration of line of sight with MEO satellites is longer with respect to LEO, and the pointing accuracy is increased, due to the lower angular velocity of the satellite, and lower influence of gravitational perturbation of the Earth's crust.

μ_{sat} estimation. The mean number of photons hitting the satellite fluctuates due to turbulence and pointing errors. This effect is evident in the deviation of the measured detection rate from the global fit. To mitigate this effect, we based the assessment of μ_{sat} not on the mean up-link attenuation but as the average number of received photons per pulse μ_{rec} divided by the downlink part of the radar equation. More specifically μ_{sat} can be obtained from

$$\mu_{rec} = \mu_{sat} \frac{\Sigma}{A_{CCR} \rho N_{eff}} \frac{1}{4\pi R^2} T_a A_t \eta_{rx} \eta_{det}, \quad (3)$$

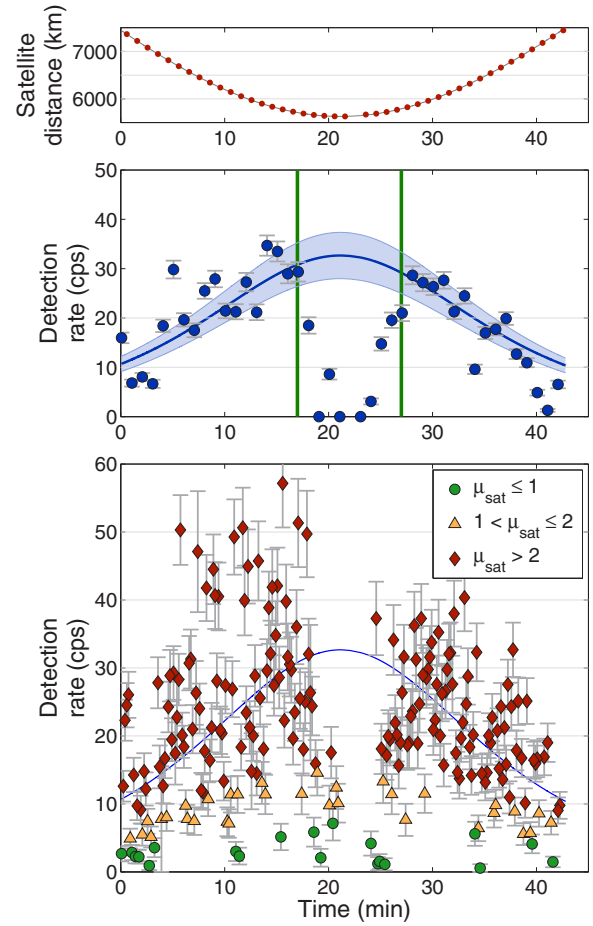


FIG. 3. Top: satellite distance to the MLRO ground station, obtained with time-of-flight measurements of SLR pulses. Middle: single-photon detection rate averaged over 60 s compared with the global fit. The shaded area represents the 99.7% of confidence level of the fit. Bottom: detection rate of single photons averaged over 10 s for different values of μ_{sat} : green circles, yellow circles, and red diamonds, respectively, correspond to $\mu_{sat} \leq 1$, $1 < \mu_{sat} \leq 2$, and $\mu_{sat} > 2$.

where $A_{CCR} = 11.4$ cm² [27] is the CCR reflective area, $\rho = 0.89$ [28] is the CCR reflectivity at normal incidence, $A_t = 1.7357$ m² is the telescope area, $\eta_{rx} = 0.1306$ is the transmission of the whole receiving apparatus, $\eta_{det} = 0.1$ is the detector efficiency, and $N_{eff} = 9.88$ [27] is the effective number of CCRs, averaged over all orientations.

To reduce the effect of the fluctuation of the pointing error on μ_{sat} estimation, we divided the whole passage in intervals of 10 s, calculating for each interval the mean μ_{rec} . With this method we computed μ_{sat} for each analysis slice, distinguishing those where $\mu_{sat} \leq 1$, $1 < \mu_{sat} \leq 2$, and $\mu_{sat} > 2$ (Fig. 3, bottom). The first two cases have a μ that can be considered practical to be used in protocols such as BB84 with decoy states [22,29]. As shown in Fig. 3, we received pulses with less than one photon per pulse when the satellite is at the largest distance from the ground station, corresponding to the maximum attenuation, and when the telescope had pointing errors, which increases the up-link losses.

By considering the intervals corresponding to $\mu_{sat} \leq 1$ it has been possible to obtain a total integration time of

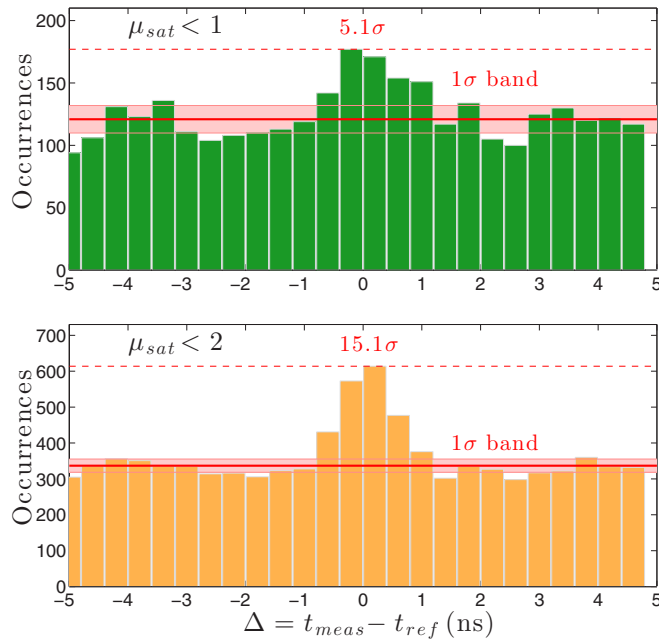


FIG. 4. Histograms of detections as a function of deviation Δ from expected time t_{ref} for different values of μ_{sat} . When only intervals with $\mu_{sat} < 1$ are selected (top), a peak is observed at $\Delta = 0$ with statistical significance over background of 5.1σ . If the analysis is extended to $\mu_{sat} < 2$ (bottom) the peak significance reaches 15.1σ . Bin size is 0.4 ns. Robustness of the peaks has been verified by changing the bin size.

200 s. For these periods we compared the time stamp of each photon detection with the nearest t_{ref} , with the same technique devised for the analysis reported in Fig. 2. As shown in the upper graph of Fig. 4, we obtained a peak with statistical significance of $(5.1 \pm 1.2)\sigma$ over background (here σ is the standard deviation of the background counts). The mean signal intensity for this interval is $\mu_{sat} = 0.55 \pm 0.06$, while the mean downlink attenuation is 72.3 dB. The average detection rate is 3.0 ± 0.3 counts/s, and the peak signal-to-noise ratio is $SNR = 1.5 \pm 0.1$.

We repeated the same analysis for intervals with $\mu_{sat} \leq 2$ (Fig. 4 bottom). This resulted in an integration period of 510 s, a statistical significance of the peak over background of $(15.1 \pm 1.3)\sigma$, a mean $\mu_{sat} = 1.19 \pm 0.05$, and a similar downlink attenuation, of 72.4 dB. The mean detection rate is 6.8 ± 0.3 counts/s and the peak $SNR = 1.8 \pm 0.1$.

Based on these observations, we extrapolate the feasibility of QC with MEO satellites by simulating the photon link budget using the best current technology of detectors (silicon-based single-photon avalanche detectors) and under the hypothesis of effectively coupling on them the satellite returns. From Ref. [30], peak detection efficiency is taken as $\eta_S = 48\%$, FWHM timing accuracy as 50 ps, and dark count rate as $DC_S \simeq 350$ counts/s. These values significantly

overpass those available for the present experiment, $\eta_{PMT} = 10\%$, $FWHM_{PMT} = 1.22$ ns, and $DC_{PMT} = 50$ counts/s, that are relative to the PMT technology, which was imposed by the current optical system coupled to the Coudé path. We note that 50 ps are compatible with the expected temporal broadening of the pulse due to propagation, which are of the order of a few picoseconds [31]. Moreover, by adopting a modulated CCR as proposed in [22] with a light amplitude modulator allowing for $\mu_{fixed} = 0.6$ during the whole satellite passage, it would be possible to enhance the detection rate by a factor $\frac{\mu_{fixed}}{\mu_{sat}} \frac{\eta_S}{\eta_{PMT}} = 5.2$ while reducing the dark count rate within the coincidence window by a factor $\frac{DC_{PMT}}{DC_S} \frac{FWHM_{PMT}}{FWHM_S} \simeq 3.45$.

Because of these steps, the SNR increases by a factor 18 with respect to the values here obtained, corresponding to a quantum bit error ratio $QBER \simeq 3.6\%$. In the hypothesis that no other effects would step in the budget [32], QKD from a MEO satellite appears feasible. For extending QC to a higher orbit such as the GNSS, between 19 000 and 23 000 km of altitude, a possible improvement of the detector dark counts down to $\simeq 100$ counts/s is necessary. In this case the signal would be reduced by a factor 10.8, due to the $1/R^2$ factor in (3), giving a value of $QBER \simeq 6.6\%$ that is compatible with the implementation of QKD for such GNSS satellites.

A possible improvement could come from the use of superconducting single-photon detectors. With nanowire superconducting technology it is possible to obtain efficiency up to 80%, dark count rates as low as 10 Hz, and time jitter of 40 ps. With these parameters it would be possible to obtain a $QBER = 0.5\%$ from a satellite with the same orbital parameters as LAGEOS, and $QBER = 3\%$ from a GNSS satellite. However, it must be noticed that the smaller sensitive area of superconductive devices, which reaches $\sim 16 \mu m$ compared to $\sim 200 \mu m$ of silicon-based detectors, might lead to a lower efficiency due to the optical coupling.

Conclusions. We report on the experimental exchange of single photons from the LAGEOS-2 satellite to the MLRO ground station, with a link length exceeding 7000 km. The photon transmission has been kept stable for most of the passage of the MEO satellite, allowing for the assessment of the signal attenuation due to beam divergence and telescope pointing error by means of the established link models. By using an active source on satellite and commercially available silicon detectors, a $QBER$ suitable for the implementation of a QKD link from a MEO satellite appears as feasible. This also paves the way to endeavoring QC with GEO satellites and eventually to fundamental tests of combined quantum mechanics and general relativity.

Acknowledgments. We would like to thank Francesco Schiavone, Giuseppe Nicoletti, and the MRLO technical operators for the collaboration and support. Our work was supported by the Strategic-Research-Project QUINTET of the Department of Information Engineering, University of Padova, and the Strategic-Research-Project QUANTUMFUTURE of the University of Padova.

[1] J. S. Bell, *Physics* **1**, 195 (1964).

[2] N. Brunner, D. Cavalcanti, S. Pironio, V. Scarani, and S. Wehner, *Rev. Mod. Phys.* **86**, 419 (2014).

[3] B. Hensen *et al.*, *Nature (London)* **526**, 682 (2015).

[4] M. Zukowski, A. Zeilinger, M. A. Horne, and A. K. Ekert, *Phys. Rev. Lett.* **71**, 4287 (1993).

- [5] X. Ma, S. Zotter, J. Kofler, R. Ursin, T. Jennewein, C. Brukner, and A. Zeilinger, *Nat. Phys.* **8**, 479 (2012).
- [6] T. Inagaki, N. Matsuda, O. Tadanaga, M. Asobe, and H. Takesue, *Opt. Express* **21**, 23241 (2013).
- [7] X. S. Ma *et al.*, *Nature (London)* **489**, 269 (2012).
- [8] V. Scarani, H. Bechmann-Pasquinucci, N. J. Cerf, M. Dušek, N. Lütkenhaus, and M. Peev, *Rev. Mod. Phys.* **81**, 1301 (2009).
- [9] C. H. Bennett and P. W. Shor, *Science* **284**, 747 (1999).
- [10] H. K. Lo and H. F. Chau, *Science* **283**, 2050 (1999).
- [11] M. Curty and D. J. Santos, *Phys. Rev. A* **64**, 062309 (2001).
- [12] T. Y. Wang, X. Q. Cai, Y. L. Ren, and R. L. Zhang, *Sci. Rep.* **5**, 9231 (2015).
- [13] B. Korzh, C. C. W. Lim, R. Houlmann, N. Gisin, M. J. Li, D. Nolan, B. Sanguinetti, R. Thew, and H. Zbinden, *Nat. Photon.* **9**, 163 (2015).
- [14] M. Aspelmeyer, T. Jennewein, M. Pfennigbauer, W. Leeb, and A. Zeilinger, *IEEE J. Sel. Top. Quantum Electron.* **9**, 1541 (2003).
- [15] C. Bonato, M. Aspelmeyer, T. Jennewein, C. Pernechele, P. Villoresi, and A. Zeilinger, *Opt. Express* **14**, 10050 (2006).
- [16] A. Tomaello, C. Bonato, V. Da Deppo, G. Naletto, and P. Villoresi, *Adv. Space Res.* **47**, 802 (2011).
- [17] J.-P. Bourgoin *et al.*, *New J. Phys.* **15**, 023006 (2013).
- [18] T. Scheidl, E. Wille, and R. Ursin, *New J. Phys.* **15**, 043008 (2013).
- [19] D. E. Bruschi, T. C. Ralph, I. Fuentes, T. Jennewein, and M. Razavi, *Phys. Rev. D* **90**, 045041 (2014).
- [20] P. Villoresi, T. Jennewein, F. Tamburini, M. Aspelmeyer, C. Bonato, R. Ursin, C. Pernechele, V. Luceri, G. Bianco, and A. Zeilinger, *New J. Phys.* **10**, 033038 (2008).
- [21] J. Yin *et al.*, *Opt. Express* **21**, 20032 (2013).
- [22] G. Vallone, D. Bacco, D. Dequal, S. Gaiarin, V. Luceri, G. Bianco, and P. Villoresi, *Phys. Rev. Lett.* **115**, 040502 (2015).
- [23] D. Rideout *et al.*, *Class. Quantum Grav.* **29**, 224011 (2012).
- [24] M. Zych, F. Costa, I. Pikovski, T. C. Ralph, and C. Brukner, *Class. Quantum Grav.* **29**, 224010 (2012).
- [25] F. Gerlin, N. Laurenti, G. Naletto, G. Vallone, P. Villoresi, L. Bonino, S. Mottini, and Z. Sodnik, in *Proceedings of the 2013 International Conference on Localization and GNSS (ICL-GNSS)* (IEEE, New York, 2013), pp. 1–6.
- [26] J. Degnan, *Geodynam. Ser.* **25**, 133 (1993).
- [27] D. A. Arnold, Optical and infrared transfer function of the Lageos retroreflector array, http://ilrs.gsfc.nasa.gov/docs/Arnold_1978.pdf.
- [28] P. O. Minott, T. W. Zagwodzki, T. Varghese, and M. Seldon, Prelaunch optical characterization of the Laser Geodynamic Satellite (LAGEOS 2), NASA technical report, http://ilrs.gsfc.nasa.gov/docs/nasa_tp3400.pdf.
- [29] T. Tsurumaru, A. Soujaeff, and S. Takeuchi, *Phys. Rev. A* **77**, 022319 (2008).
- [30] A. Giudice, M. Ghioni, R. Biasi, F. Zappa, S. D. Cova, P. Maccagnani, and A. Gulinatti, *J. Mod. Opt.* **54**, 225–237 (2007).
- [31] J. W. Marini and C. W. Murray, Correction of laser range tracking data for atmospheric refraction at elevations above 10 degrees, Greenbelt, MD: Goddard Space Flight Center, NASA Technical Report, NASA-TM-X-70555, X-591-73-351 (1973).
- [32] J. Bae and A. Acín, *Phys. Rev. A* **75**, 012334 (2007).